# Electronic supplementary information (ESI)

## Multiresponsive luminescent sensing behaviour of a tetraimidazole ligand and its 3D Cd(II) metal-organic frameworks

Ye-Feng Wu, Jia-Jun Cheng, Tao Jiang, Yu-Chen Ma, Jia-Lei Kou, Guo-Feng Cheng, Xiu-Li Hu, Xiao-Yan Tang, Yun-Sheng Ma*, Wen-Yu Yin* and Hong-Jian Cheng*

*School of Materials Engineering, Changshu Insititute of Technology, Changshu, Jiangsu, 215500, P. R. China.*

**Contents**

***Preparation of timpb***

A 10 mL deep porcelain crucible was filled with a mixture of 2.24 g (5.0 mmol) 1,3-dibromo-5-(3,5-dibromo-phenoxymethyl)-benzene, 6.808 g (100.0 mmol) imidazole, 4.146 g (30.0 mmol) anhydrous potassium carbonate and 0.380 g (2.0 mmol) cuprous iodide. The reaction mixture was exposed to microwave irradiation at different temperatures and times. After cooling to room temperature, the residue was diluted with 20 mL $H_2O$. 0.292 g (1 mmol) ethylenediaminetetraacetic acid and 4 mL $NH_3 \cdot H_2O$ (28-29 %) was added, and the resulting mixture was stirred at room temperature for 24 h. The resulting dark brown precipitate was filtered and further purified by recrystallization in methanol to form light gray powder of timpb. Yield: 1.137 g (76 %). Anal. Calcd for $C_{25}H_{20}N_8O$: C 66.95; H 4.49; N 24.99; found C 67.34; H 4.36; N 24.26. IR (KBr, $cm^{-1}$): 3098(w), 1654(m), 1509(s), 1475(w), 1399(m), 1340(m), 1247(w), 1111(w), 1058(m), 960(w), 912(w), 829(m), 730(m), 525(m). $^1H$ NMR (DMSO-$d_6$, 400 MHz, ppm) δ 8.47 (s, 4H), 8.01 (s, 1H), δ 7.95 (s, 3H), 7.83 (s, 2H), 7.64 (s, 1H), δ 7.43 (s, 2H), 7.18 (s, 3H), 5.37 (s, 2H).

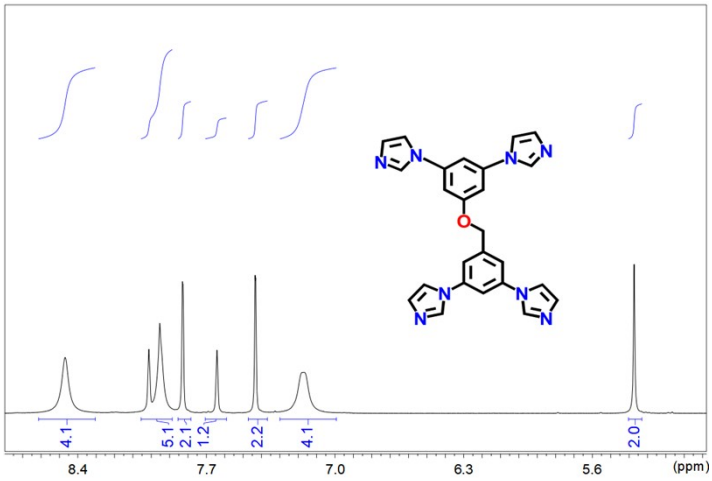


**Fig. S1.** $^1H$ NMR spectra of timpb.

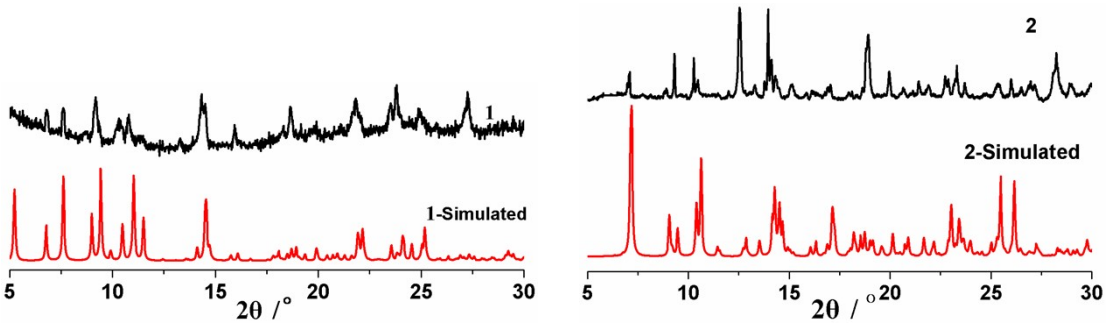


(a) (b)

**Fig. S2.** PXRD patterns for **1** and **2**. simulated (red) and single-phase polycrystalline (black) sample of **1** or **2**.

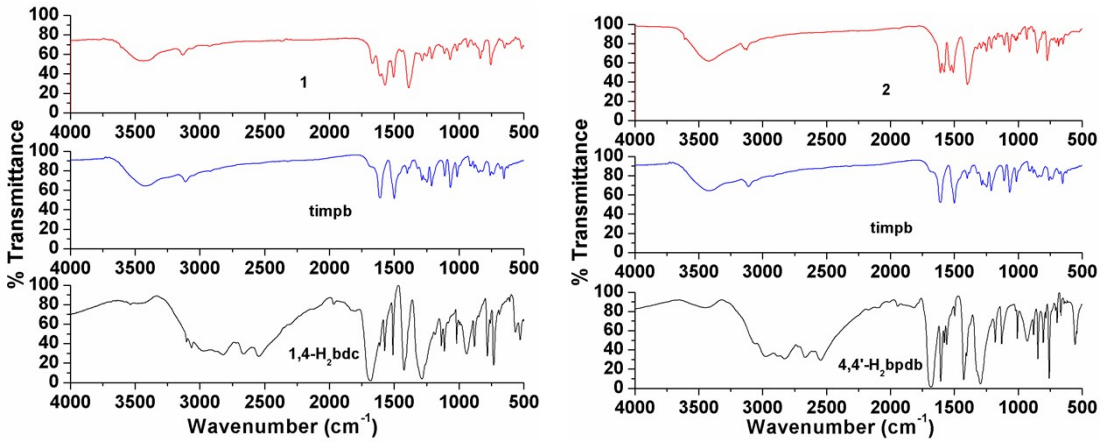


(a) (b)

**Fig. S3** (a) FT-IR spectra of **1** with timpb and 1,4-$H_2$bdc; (b) FT-IR spectra of **2** with timpb and 4,4′-$H_2$bpdb.

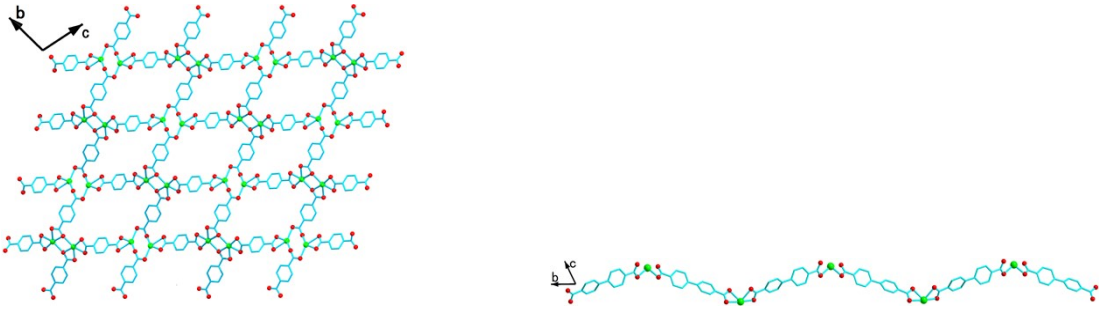


（a） (b)

**Fig. S4** (a) 2D net constructed by [Cd(1,4-bdc)] units in **1** (looking down the *a* axis); (b) 1D chain constructed by [Cd(4,4'-bpdb)] units in **2** (looking down the *a* axis).

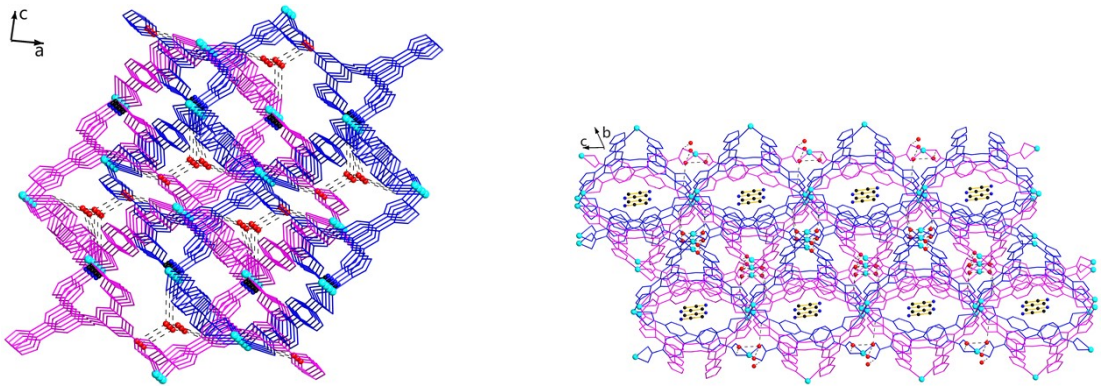


(a) (b)

**Fig. S5** The 3D struture of **2** containing solvent molecules looking down the *b* axis (a) or the *a* axis.

**Table S1.** Selected bond lengths (Å) and angles (°) of **1** and **2**

| | | | |
|---|---|---|---|
| **Complex 1** | | | |
| Cd(1)-N(1) | 2.269(6) | Cd(1)-N(5)#1 | 2.303(6) |
| Cd(1)-O(6) | 2.303(6) | Cd(1)-O(7)#2 | 2.321(6) |
| Cd(1)-O(2) | 2.351(6) | Cd(1)-O(3) | 2.528(7) |
| Cd(2)-N(3) | 2.266(7) | Cd(2)-N(7)#3 | 2.283(6) |
| Cd(2)-O(9)#4 | 2.343(6) | Cd(2)-O(4)#5 | 2.365(6) |
| Cd(2)-O(8)#2 | 2.372(6) | Cd(2)-O(5)#5 | 2.458(6) |
| Cd(2)-O(9)#2 | 2.553(6) | | |
| N(1)-Cd(1)-N(5)#1 | 174.9(2) | N(1)-Cd(1)-O(6) | 101.1(2) |
| N(5)#1-Cd(1)-O(6) | 82.2(2) | N(1)-Cd(1)-O(7)#2 | 91.8(2) |
| N(5)#1-Cd(1)-O(7)#2 | 83.1(2) | O(6)-Cd(1)-O(7)#2 | 121.66(19) |
| N(1)-Cd(1)-O(2) | 91.9(2) | N(5)#1-Cd(1)-O(2) | 92.1(2) |
| O(6)-Cd(1)-O(2) | 89.3(2) | O(7)#2-Cd(1)-O(2) | 147.3(2) |
| N(1)-Cd(1)-O(3) | 90.2(2) | N(5)#1-Cd(1)-O(3) | 89.7(2) |
| O(6)-Cd(1)-O(3) | 141.0(2) | O(7)#2-Cd(1)-O(3) | 94.8(2) |
| O(2)-Cd(1)-O(3) | 52.75(18) | N(3)-Cd(2)-N(7)#3 | 174.2(2) |
| Cd(1)-N(1) | 2.269(6) | Cd(1)-N(5)#1 | 2.303(6) |
| **Complex 2** | | | |
| Cd(1)-O(3) | 2.201(4) | Cd(1)-O(7) | 2.215(4) |
| Cd(1)-N(1) | 2.246(4) | Cd(1)-N(8)#1 | 2.251(5) |
| Cd(2)-N(3) | 2.258(4) | Cd(2)-O(5)#2 | 2.270(4) |
| Cd(2)-N(5)#3 | 2.293(5) | Cd(2)-O(8)#4 | 2.354(4) |
| Cd(2)-O(9)#4 | 2.370(4) | Cd(2)-O(4)#2 | 2.471(4) |
| O(3)-Cd(1)-O(7) | 104.79(15) | O(3)-Cd(1)-N(1) | 95.35(16) |
| O(7)-Cd(1)-N(1) | 131.90(15) | O(3)-Cd(1)-N(8)# | 132.16(17) |
| O(7)-Cd(1)-N(8)#1 | 90.54(16) | N(1)-Cd(1)-N(8)#1 | 107.49(17) |
| N(3)-Cd(2)-O(5)#2 | 96.82(17) | N(3)-Cd(2)-N(5)#3 | 107.58(18) |
| O(5)#2-Cd(2)-N(5)#3 | 91.73(16) | N(3)-Cd(2)-O(8)#4 | 136.84(17) |
| O(5)#2-Cd(2)-O(8)#4 | 119.01(15) | N(5)#3-Cd(2)-O(8)#4 | 95.32(16) |
| N(3)-Cd(2)-O(9)#4 | 88.09(15) | O(5)#2-Cd(2)-O(9)#4 | 174.23(15) |
| N(5)#3-Cd(2)-O(9)#4 | 89.65(16) | O(8)#4-Cd(2)-O(9)#4 | 55.26(13) |
| N(3)-Cd(2)-O(4)#2 | 94.73(17) | O(5)#2-Cd(2)-O(4)#2 | 55.28(15) |
| N(5)#3-Cd(2)-O(4)#2 | 142.58(16) | O(8)#4-Cd(2)-O(4)#2 | 87.75(14) |
| O(9)#4-Cd(2)-O(4)#2 | 121.46(15) | | |

[a] Symmetry codes: for **1**: #1 x + 1, y – 1, z; #2 – x + 2, – y, – z + 1; #3 x + 1, y, z + 1; #4 x, y + 1, z + 1; #5 – x + 1, – y, – z + 2.

For **2**, #1 x – 1, y, z; #2 x + 1, y – 1, z + 1; #3 x, y + 1, z; #4 x, y + 1, z + 1; #5 x – 1, y + 1, z – 1; #6 x, y – 1, z – 1; #7 x, y – 1, z; #8 x + 1, y, z

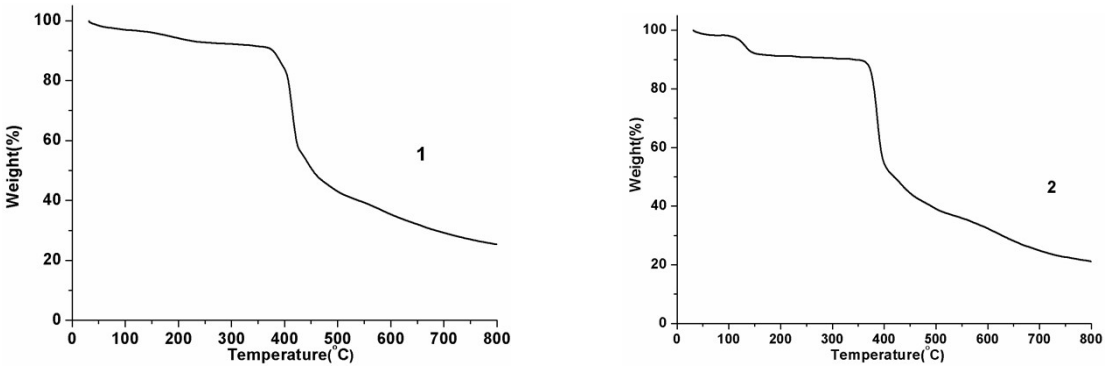


(a) (b)

**Fig. S6** (a) The TGA curves for **1**; (b) The TGA curves for **2**.

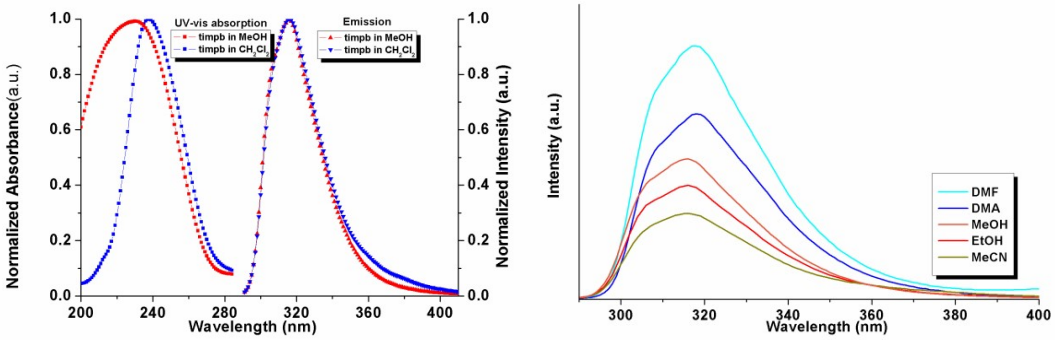


(a) (b)

**Fig. S7** (a) UV-visible absorbance (left) and emission spectra (right) of timpb in dilute mathanol or dichlorom solutions ($1 \times 10^{-4}$ mg $mL^{-1}$); (b) Fluorescence emission spectra of timpa in different organic solvents.

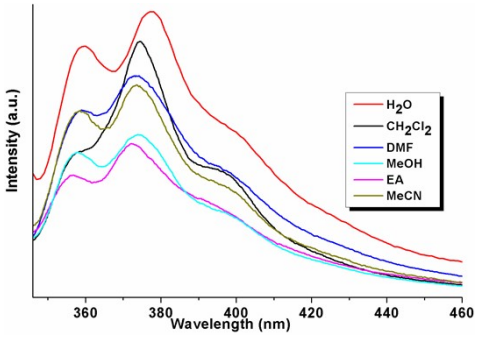


**Fig. S8** Fluorescence emission spectra of **1** in different organic solvents.

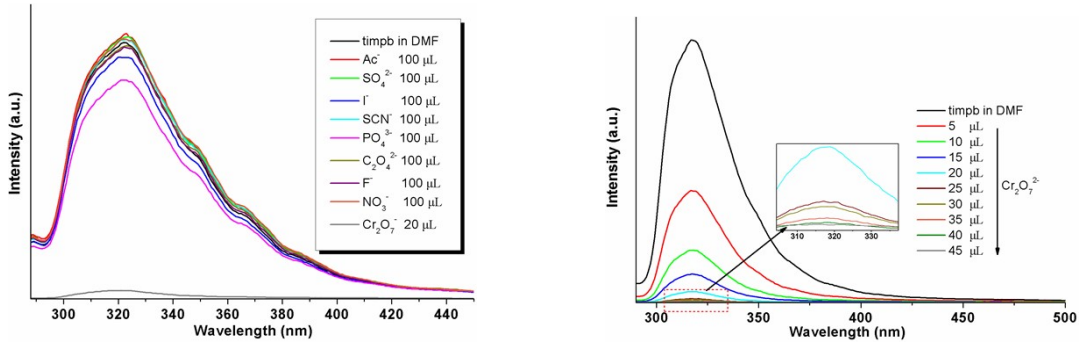


(a) (b)

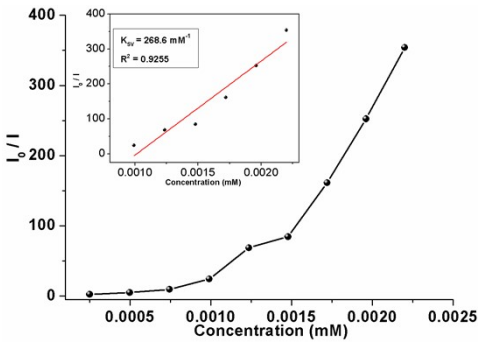


(c)

**Fig. S9** (a) Fluorescent sensing responses of timpb ($10^{-6}$ M) upon addition of 100 μL of various anions ($10^{-4}$ M) in water; (b) Fluorescence titration profile of timpb ($10^{-6}$ M) with successively increasing concentration of $Cr_2O_7^{2-}$ ions ($10^{-4}$ M) from 5 to 45 μL; (c) $K_{sv}$ plot of timpb for sensing of $Cr_2O_7^{2-}$ (inset: the linear correlation at higher concentrations).

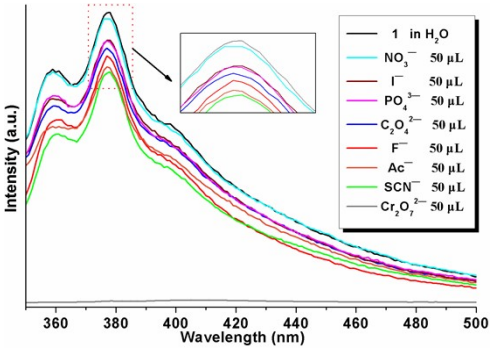


(a)

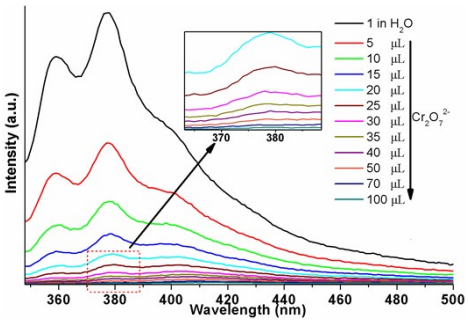


(b)

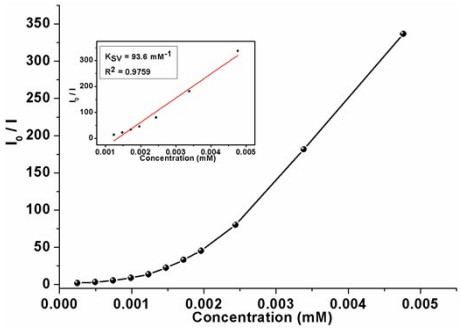


(c)

**Fig. S10** (a) Fluorescent sensing responses of **1** upon addition of 50 μL of various anions ($10^{-4}$ M) in water; (b) Fluorescence titration profile of **1** with successively increasing concentration of $Cr_2O_7^{2-}$ ions ($10^{-4}$ M) from 5 to 100 μL; (c) $K_{sv}$ plot of **1** for sensing of $Cr_2O_7^{2-}$ (inset: the linear correlation at higher concentrations).

**Table S2.** Comparison of the detection limits of previously reported sensors with our work for the detection of $Cu^{2+}$, $Fe^{3+}$ or $Cr_2O_7^{2-}$ ions

| Sensor | ions | LOD | Ref. |
|---|---|---|---|
| Acetylenic-indole conjoined organosilatrane | $Cu^{2+}$ | 0.41 μM | 33a |
| Graphene quantum dots | $Cu^{2+}$ | 0.226 μM | 33b |
| Rhodamine spirolactam derivative | $Cu^{2+}$ | $3 \times 10^{-4}$ μM | 33c |
| Inclusion complex with β-cyclodextrin and 1,5-Dihydroxyanthraquinone | $Cu^{2+}$ | 10 nM | 33d |
| | $Cr_2O_7^{2-}$ | 0.8 nM | |
| 4-bromo-2-hydroxyben Rhodamine B hydrazide | $Cu^{2+}$ | $1.7 \times 10^{-4}$ μM | 33e |
| Zn(II)-MOFs | $Fe^{3+}$ | $2.75 \times 10^{-3}$ μM | 34a |
| | $Cr_2O_7^{2-}$ | $4.43 \times 10^{-4}$ μM | |
| $\{[Eu(L)(H_2O)]\cdot 7H_2O\}_n$ | $Fe^{3+}$ | 0.67 μM | 34b |
| $H_3L$ = 5-(3′,5′-dicarboxylphenyl)picolinic acid | $Cr_2O_7^{2-}$ | 0.32 μM | |
| $\{[(CH_3)_2NH_2]_4[Ca_2Zn_4(L)_4]\cdot 4DMF\}_n$ | $Fe^{3+}$ | 18.8 μM | 34c |
| $H_4L$ = 5,5′-(propanen-1,3-diyl)-bisIJoxy)diisophthalic acid | $Cr_2O_7^{2-}$ | 29.1 μM | |
| $Eu^{3+}$@MIL-124 | $Fe^{3+}$ | 0.28 μM | 34d |
| 2,2′-bisbenzimidazole derivative | $Fe^{3+}$ | $1.0 \times 10^{-6}$ μM | 34e |
| $\{[Cu(L)_2(H_2O)_2]\cdot(SiF_6)(H_2O)\}_n$ | $Cr_2O_7^{2-}$ | 0.79 μM | 35a |
| L = 4,4′-azobispyridine | | | |
| $\{[Zn_2(\mu_3\text{-}OH)(cpta)(4,4'\text{-}bipy)]\cdot H_2O\}_n$ | $Cr_2O_7^{2-}$ | $6.91 \times 10^{-3}$ μM | 35b |
| $H_3cpta$ = 2–(-carboxyphenoxy)terephthalic acid | | | |
| $[Ln(TCPB)(DMF)_3]_n$ | $Cr_2O_7^{2-}$ | $3.0 \times 10^{-4}$ μM | 35c |
| $H_3TCPB$ = 1,3,5-tris(1-(2-carboxyphenyl)-1H-pyrazol-3-yl) | | | |
| $[Cd(TPA)(BIYB)]_n$ | $Cr_2O_7^{2-}$ | $2.4 \times 10^{-4}$ μM | 35d |
| $H_2TPA$ = 3,3′-thiodipropionic acid | | | |
| BIYB = 4,4-bis(imidazol-1-ylmethyl)biphenyl | | | |
| Water-soluble carbon dots | $Cr_2O_7^{2-}$ | 140 nM | 35e |
| $\{[Tb(dppa)(H_2O)_2]\cdot dima\cdot H_2O\}_n$ | $Cr_2O_7^{2-}$ | 0.55 μM | 35f |
| $H_4dppa$ = 5-(3′, 4′-dicarboxylphenoxy)isophthalic acid | | | |
| dima = dimethylamine | | | |

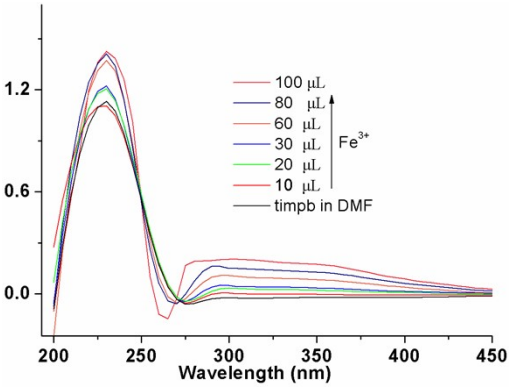


(a)

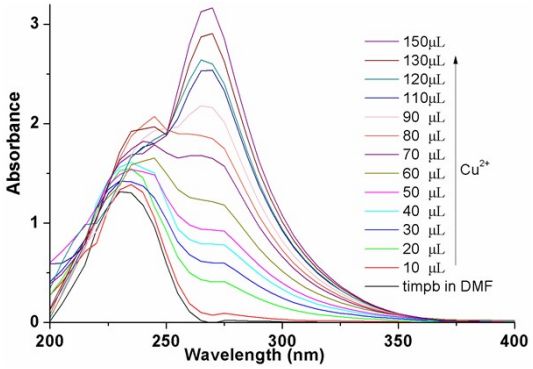


(b)

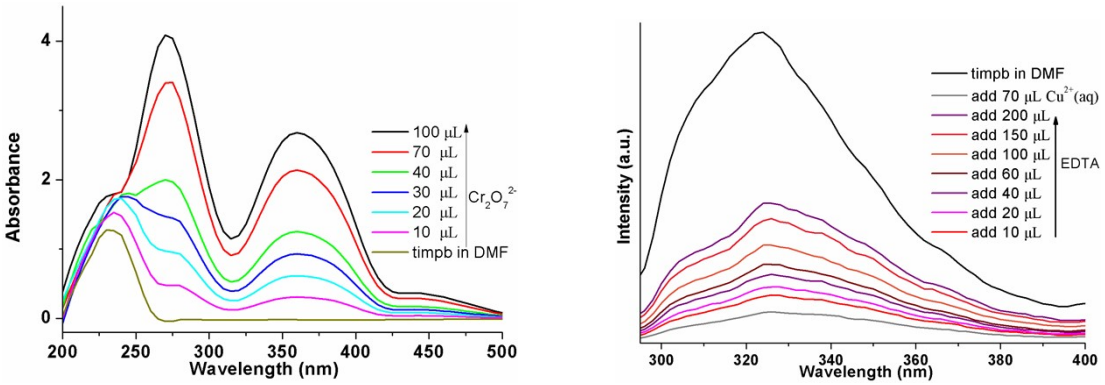


(b) (d)

**Fig. S**11 (a) UV-visible absorbance spectra of timpb ($10^{-6}$ M) with successively increasing concentration of $Fe^{3+}$ ions ($10^{-4}$ M) from 10 to 100 μL; (b) UV-visible absorbance spectra of timpb ($10^{-6}$ M) with successively increasing concentration of $Cu^{2+}$ ions ($10^{-4}$ M) from 10 to 150 μL; (c) UV-visible absorbance spectra of timpb ($10^{-6}$ M) with successively increasing concentration of $Cr_2O_7^{2-}$ ions ($10^{-4}$ M) from 10 to 100 μL; (d) Fluorescent recovery responses of 2 mL timpb ($10^{-6}$ M) + 70 μL $Cu^{2+}$ ions ($10^{-4}$ M) upon addition of EDTA ($10^{-4}$ M).

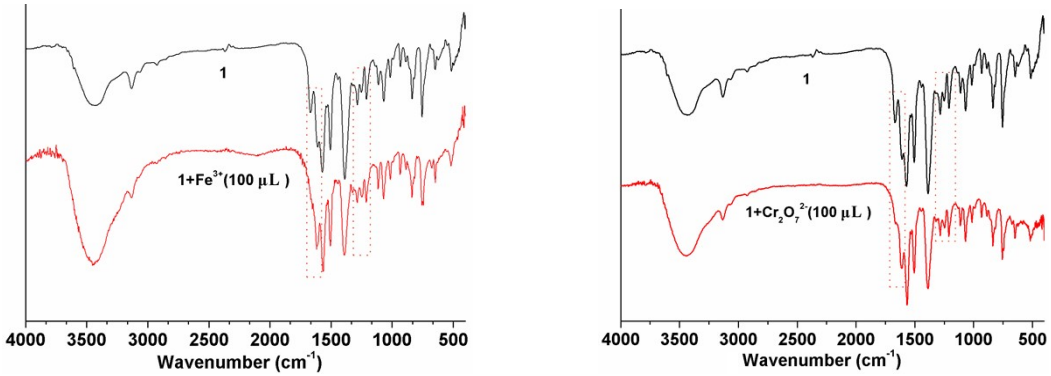


(a) (b)

**Fig. S12** FTIR spectra of **1** before and after sensing concentrations of $Fe^{3+}$ (a) and $Cr_2O_7^{2-}$ (c) at room temperature.

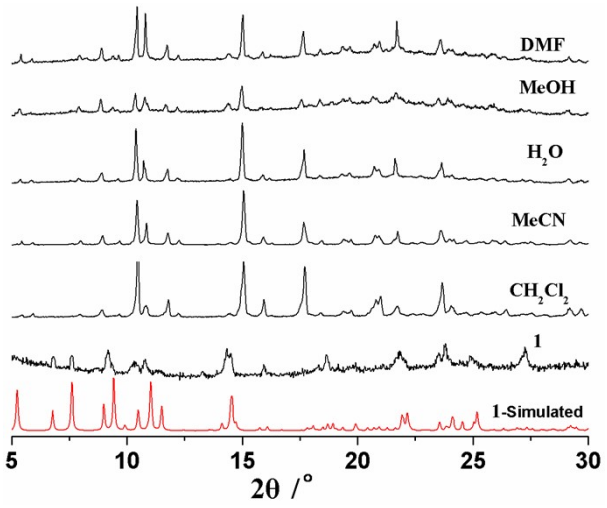


**Fig. S13** PXRD patterns exhibited by complex **1** after immersion in various solvents for 3 days.

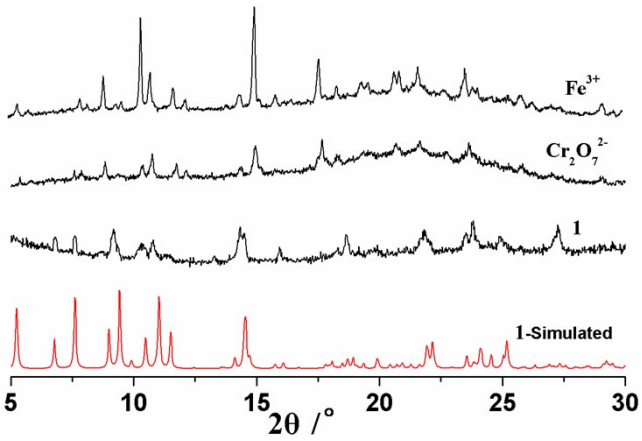


**Fig. S14** PXRD patterns exhibited by complex **1** after immersion in aqueous solutions containing $Fe^{3+}$ or $Cr_2O_7^{2-}$.

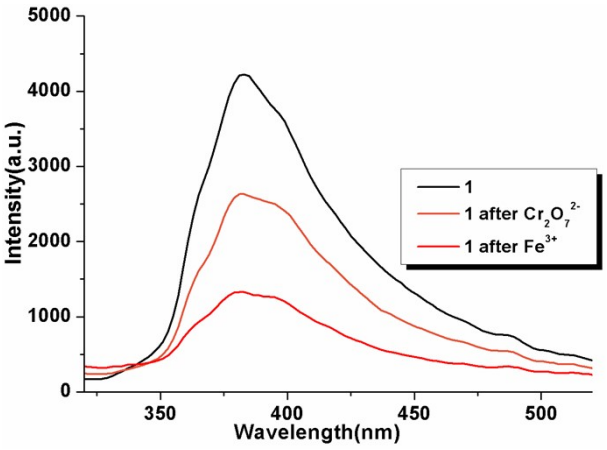


**Fig. S15** The emission spectra of **1** in the solid state after immersion in aqueous solutions containing $Fe^{3+}$ or $Cr_2O_7^{2-}$.